Optica Applicata, Vol. LIV, No. 3, 2024
DOI: 10.37190/oa240302

New possibilities of polarization-sensitive optical coherence tomography using geometric phase approach for diagnostics of thin surface (subsurface) biological layers

Claudia ZENKOVA[1,2,*], Oleg ANGELSKY[1,2], Dmytro IVANSKYI[2]

[1]Research Institute of Zhejiang University, Taizhou City, Zhejiang Province, 318000 China

[2]Chernivtsi National University, 2 Kotsyubinsky St., Chernivtsi 58012, Ukraine

[*]Corresponding author: k.zenkova@chnu.edu.ua

The paper focuses on presenting the new original results and highlighting of possibilities of geometric phase using in low-coherence polarization-sensitive tomography tasks for noninvasive diagnostics of surface (subsurface) layers of transparent (translucent) biological media (samples and tissues). Determination of the object fields' geometric phase in the modified Mach–Zehnder interferometer allows one to reproduce the geometric structure (optical axis/collagen orientation) of birefringent biological medium. Polarization-interference noninvasive approach of the collagen orientation structure diagnostics of thin nanosized surface tissue layers is proposed at the first time. It is shown, that taking into account the information about top (surface) layer structure can significantly improve the accuracy of deeper (subsurface) layers parameters estimation. The proposed solution is a unique feature that is not accessible in classical polarization-sensitive techniques of information recovery on tissue structure.

Keywords: polarization-sensitive optical coherence tomography, geometric phase, anisotropic biological tissue, surface (subsurface) layers, birefringence, optical axis orientation.

1. Introduction

The last century, it was proposed to use the principles of low-coherence interferometry to obtain tomographic images of biological tissues with high spatial resolution [1,2]. This approach is known as optical coherence tomography (OCT), which has opened new horizons in several fields of medical research, particularly in ophthalmology and dermatology [1-4].

The principles of OCT are based on the use of properties of biological tissues, which differ in optical density, differently reflect the light signal directed at them.

Optical coherence tomography (OCT) [1,2] achieves spatial image resolution at depths of 1–15 μm. Generally, the level of temporal coherence determines the longitudinal (axial) resolution, and the angular sizes of the source set the transverse (lateral) resolution of the system.

While reviewing the shortcomings of OCT as a method of tomography of transparent and translucent media by registering backscattered radiation, it can be noted that they are related to the lack of possibility to directly differentiate different tissues or objects, separate layers of the object, and especially in the situation when the mentioned tissue elements are damaged, displaced or destroyed. To overcome these limitations, in addition to measurements related to signal intensity estimation, it is important to carry out polarization measurements using polarization sensitive OCT – PS-OCT [3,4]. A feature of PS-OCT is that the implementation of this method makes it possible to extract information about the polarization state of the object-based optical field by examining the interference pattern.

However, PS-OCT as other OCT techniques does not provide the opportunity to visualize the surface (subsurface) areas of biological tissues or other objects, thickness of which is much less than the longitudinal resolution of the system. To perform PS-OCT beneath the surface of the object under study, endoscopy and needle-based tomography were developed. In this case, minimally invasive techniques are generally used, which involve some damage to the surface of the sample [5]. Thus, it is reasonable to search for new approaches that provide the possibility to detect small axial displacements, collagenous structure destroying (damages or scratches) the surface layers in the sample by applying noninvasive methods. Therefore, it is possible to achieve a higher signal-to-noise ratio, improving the accuracy of reconstruction the polarization and geometrical structure of the whole object.

Polarization changes due to propagation of polarized light through an optically anisotropic medium manifest themselves in arising of the geometric phase [6-8], in addition to the conventional (dynamic) phase related with the optical path length. Geometric phase depends on the initial polarization state of probing beam and is determined by the medium polarization properties, such as birefringence (phase retardation), optical axis orientation or dichroism [6]. Thus, the geometric phase of the object field serves as an additional tool for reconstruction the medium polarization parameters, providing the possibility for study thin surface (subsurface) layers.

For the solution of mentioned above problem, the use of polarization-interference approach that involves recovery of the object fields' geometric phase in one of the modified Mach–Zehnder interferometer [7] arms, was proposed. Using linear input polarization beam makes it possible to obtain the interferometric signal with the influence of geometric phase only in one of two orthogonal polarization channels. In this way, it is possible to ensure the opportunity to study the structure of surface and subsurface layers, recovering the medium parameters from geometric phase, and improving the accuracy of reproducing the structure of anisotropic biological sample in the whole.

2. Structure and properties of a birefringent biological object

As an object of study, we choose a birefringent biological object, which is the cornea of the eye, the main structural element of which is a lamella – a plane of collagen fibers. The lamellae vary in size from 0.5 to 250 μm in width and 0.2 to 2.5 μm in thickness, depending on the type [9]. Collagen fibers of corneal lamella are described by the refraction index $n_{\text{coll}} = 1.415$ and are in the medium of the basic substance with refractive index $n_{\text{base}} = 1.356$ [10]. The fibers are uniform across the diameter cross-section and are arranged in the same direction. The diameter of the collagen fiber is a value on the order of 30.8 nm and the average distance between fibers is 55.3 nm.

According to its optical properties, the cornea is transparent to visible and infrared radiation, which is explained by interference damping of secondary waves scattered by collagenous fibers backward and amplification of those scattered forward [11]. In studying the lamella within the framework of tomography approaches, the features of radiation reflected from the interfaces between separate lamellae are analyzed. In the first approximation, the presence of scattering centers (keratocytes) localized between the layers of lamellae is not considered.

In general, each lamella is a birefringent structure, that is characterized by form anisotropy [10, 12]. According to the existing model of the eye cornea [12], individual lamella can be considered as an uniaxial waveplate for that the optical axis is oriented parallel to the direction of the collagen fibers. The observed birefringence of the lamella is a linear form birefringence, which is positive because the fibers are contained in a medium with a lower refractive index. The value of birefringence [10]:

$$\Delta n = n_{\text{e}} - n_{\text{o}} = \frac{(n_{\text{coll}}^2 - n_{\text{base}}^2)(n_{\text{coll}} + n_{\text{base}})v(1-v)}{(1+v)n_{\text{coll}}^2 + (1-v)n_{\text{base}}^2} \tag{1}$$

where v – collagen fibers volume content, n_{o}, n_{e} – refractive indices of ordinary and extraordinary rays. Here $v = 0.32$ [10], $\Delta n = 0.0253$.

The average value of the refractive index is [10]: $\overline{n} = v n_{\text{coll}} + (1-v) n_{\text{base}}$. Then $\overline{n} = 1.375$, which corresponds to the literature data [11].

As a model object we chose the individual lamella in the form of a birefringent plate, of 2 μm in thickness, the orientation of the optical axis in which is identified with a main orientation of collagen fibers. The surface (subsurface) layers of lamella are considered as modified (changed, damaged, scratched) collagenous structure on its top and unchanged structure in its depth [13]. Firstly, we consider the case of unchanged lamella structure and provide the description of geometric phase approach for reconstruction of its' properties, and then consider the case when the surface layer is damaged.

Object of study determines the effective working wavelength and spectral bandwidth for the possibility of sample scanning. The working wavelength of the Ti:sapphire

laser used in ophthalmology is 850 nm with a spectral half-bandwidth of about 170 nm. Thus the axial resolution of PS-OCT system [1-4] can be determined as

$$\delta z = l_c = \frac{2\ln 2}{\pi}\frac{\lambda^2}{\Delta\lambda} = 1.87\ \mu\text{m} \tag{2}$$

which is associated with the average lamella thickness (2 μm), and the lateral resolution

$$\delta x = \sqrt{2\ln 2}\,\frac{\lambda_0}{\pi \cdot \text{NA}} = 10\ \mu\text{m} \tag{3}$$

for NA = 0.18.

3. Geometric phase approach for determination the polarization structure of the transparent (translucent) biological object

As an interference technique, PS-OCT uses different polarization channels, that carries information about the amplitude and phase of the field under study. The need for diagnostics of surface and subsurface layers of transparent (translucent) samples by non-invasive methods requires increasing the accuracy of PS-OCT measurements, especially in a case of nanosized layers, thickness of which is much less than the longitudinal resolution of a system. This actually determines the purpose of the study, the results of which are presented in this paper.

The efficiency of using the geometric phase, in an interference experiment is given by the fact that with a cyclic change of polarization in one of the arms of an interferometer, say, a modified Mach–Zehnder interferometer, the path difference of the interfering waves remains unchanged [7,14,15]. This suggests that in this case there is no contribution of the dynamic phase to the shift of the interference fringes at the output of the interferometer.

We consider the evolution of polarization states that occur during the propagation of the beam through a biological transparent (translucent) object until the interference of the object and reference beam. This evolution is depicted on the Poincaré sphere [6] as a closed loop, which allows the calculation of the geometric phase. The initial and final states differ by a phase factor equal to half the solid angle encompassed by the loop on the Poincaré sphere along which the polarization changes [6,16].

Thus, in our study and analysis we propose to detect the geometric phase in a modified Mach–Zehnder interferometer, such as the one presented in [7,14,15]. The scheme of the model experiment is presented in Fig. 1. We will assume that the biological birefringent object under study is placed in one of the arms of interferometer, and interference signals are registered in two orthogonal polarization channels – horizontal by the detector D1 and vertical by the detector D2 (Fig. 1). According to the described model of biological sample (S), we take the lamella as an optically uniaxial structure with certain values refractive index $\overline{n}$ and bierfringence Δn. The lamella itself is sur-

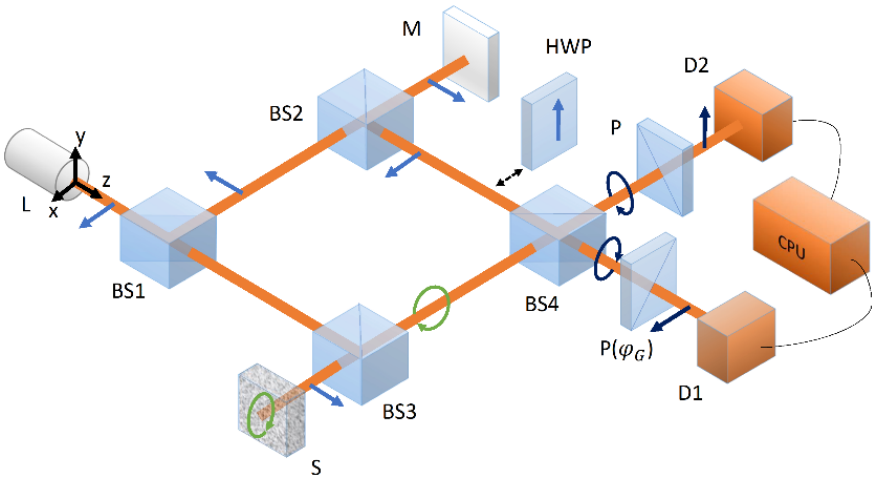

Fig. 1. The modified Mach–Zehnder interferometer scheme: L – radiation source; BS1, BS2, BS3, BS4 – nonpolarizing beamsplitters; M – mirror; HWP – half-wave plate; D1, D2 – photodetectors; CPU – computer unit; $P(\varphi_G)$ – polarizer in the horizontal channel allowing to restore the initial horizontal polarization of the beam, which makes it possible to estimate the geometric phase; P – polarizer in the vertical channel, allowing to recover the vertical component of the signal. Blue arrows show the evolution of polarization states of the reference beam, green ellipses indicate the evolution of polarization states of object beam, dark-blue ellipses describe the results of the superposition of reference and object beams, dark-blue arrows determine the results of $x(y)$ components interference. x, y, z – laboratory coordinate frame, connected with the beam propagation direction.

rounded by the biological medium (base substance), *i.e.*, the refractive index of the lamella will be greater than the refractive index of the surrounding medium ($\overline{n} > n_{\text{base}}$).

In general, in PS-OCT, a set of polarization states is used, including linear and circular ones. Here, to study the model of reproduction of information about the object geometry, we form a linear polarization of the beam, which will be sufficient for understanding of the concept. Thus, a linearly polarized beam is used, horizontally (perpendicular to the plane of incidence),

$$\mathbf{E}_0 = \begin{pmatrix} E_{0x} \\ E_{0y} \end{pmatrix} = \begin{pmatrix} 1 \\ 0 \end{pmatrix} \tag{4}$$

with the azimuth of polarization of 0° (Fig. 1).

The essence of the proposed model approach is that a horizontal linear polarization is recovered in the horizontal channel behind the polarizer $P(\varphi_G)$, and repeats the polarization state in front of BS1 at the input of the interferometer (Fig. 1). The corresponding polarization states obtained during propagation of the object beam are marked on the Poincaré sphere. Thus, it is possible to obtain the closed loop, which allows us to retrieve information about the geometric phase.

The intensity measurement is carried out in both horizontal and vertical arms of the interferometer. Information about two orthogonal components (amplitude and

phases) of the polarization ellipse of the object beam ($\mathbf{E}_{\mathrm{Ob}}$) is extracted from the horizontal and the vertical arms of the interferometer.

The nonpolarizing beamsplitters (BS1–BS4) perform the function of dividing the intensity of the incident beam in the transmission and reflection directions in the ratio of 50/50, equally redistributing the beams through the two channels. When the beams are reflected at the beamsplitters, the phase of the reflected beam changes and the polarization state also changes. The change of phase and polarization state of the beams is manifested (Fig. 1) and taken into account during construction of the polarization ellipses.

After the BS1, the beam propagating towards the BS3, which is responsible for the formation of the object wave, is reflected from it in the direction to the object. Reflected wave acquires a phase jump at π, and remains linearly polarized, but with a Jones vector $\mathbf{E}_0' = \begin{pmatrix} 1 \\ 0 \end{pmatrix}$ (Fig. 2). A birefringent medium (object), of thickness d, sets the phase delay ($\delta = k\,\overline{n}\,d$, here $\overline{n} = (n_{\mathrm{o}} + n_{\mathrm{e}})/2$ – average refractive index of the medium, $k = 2\pi/\lambda$), between the two arms of the interferometer, and this delay is determined by the doubling of the incident beam path length.

In this paper, we use the following model. As an object we consider the eye cornea lamella with a thickness $d = 2$ μm (Fig. 2). The object is placed in a medium with a lower refractive index (n_{base}). In a first approximation, we consider that collagenous structure distribution is uniform along all the depth of lamella (Fig. 2(a)). We provide the geometric phase approach to extract the information about the orientation of these collagen fibers. In the second case we assume that the collagenous structures in the upper (surface) layer of lamella (d_1) are changed in their orientation due to the destroy of sample (Fig. 2(b)), and the deeper (subsurface) (d_2) layer remains unchanged.

So, firstly we consider the formation of the object beam due to the reflection from the inner interface of the unchanged lamella (Fig. 2(a)).

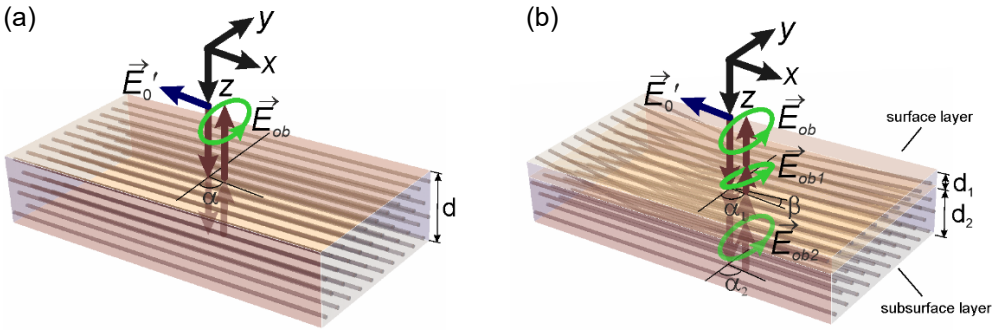

Fig. 2. Formation of the object beam polarization ellipse in a case of: (a) normal (unchanged) lamella (α determines the orientation of optical axis (collagen fiber) with respect to the horizontal direction); (b) surface and subsurface layers of modified lamella. α_1 (α_2) – angles of the orientation of optical axis (collagen fiber) in a plane of unchanged (changed) lamella surfaces with respect to the horizontal direction, β – rotation angle of the destroyed lamella surface relative to the normal lamella subsurface. $\mathbf{E}_0'$ – incident beam, $\mathbf{E}_{\mathrm{Ob}}$ – object beam, $\mathbf{E}_{\mathrm{Ob1,2}}$ – object beams after the reflection from inner surface of the two layers.

Jones matrix of the birefringent object is [17]:

$$\mathbf{M} = \mathrm{e}^{i\delta}\begin{pmatrix} \cos\frac{\gamma}{2} + i\sin\frac{\gamma}{2}\cos 2\alpha & i\sin\frac{\gamma}{2}\sin 2\alpha \\ i\sin\frac{\gamma}{2}\sin 2\alpha & \cos\frac{\gamma}{2} - i\sin\frac{\gamma}{2}\cos 2\alpha \end{pmatrix} \tag{5}$$

In a Jones matrix of a birefringent object, two main polarization parameters of the medium are taken into account – geometry (orientation of optical axis α with respect to horizontal direction, Fig. 2(a)), phase retardation $\gamma = kd(n_\mathrm{e} - n_\mathrm{o})$, and δ value related to the properties of the medium.

After interaction with the object, reflection from the inner surface of the object, and propagation in the backward direction, the beam will be elliptically polarized, and the Jones vector of which $\mathbf{E}_\mathrm{Ob}$ will be [8]:

$$\mathbf{E}_\mathrm{Ob} = \begin{pmatrix} E_{\mathrm{Ob}_x} \\ E_{\mathrm{Ob}_y} \end{pmatrix} = \mathbf{M}\cdot\mathbf{M}\cdot\mathbf{E}_0' = -\mathrm{e}^{2i\delta}\begin{pmatrix} \cos\gamma + i\sin\gamma\cos 2\alpha \\ i\sin\gamma\sin 2\alpha \end{pmatrix} = \begin{pmatrix} A_{\mathrm{Ob}_x}\mathrm{e}^{i\varphi_{\mathrm{Ob}x}} \\ A_{\mathrm{Ob}_y}\mathrm{e}^{i\varphi_{\mathrm{Oby}}} \end{pmatrix} \tag{6}$$

Here $A_{\mathrm{Ob}x}$, $A_{\mathrm{Ob}y}$, $\varphi_{\mathrm{Ob}x}$, $\varphi_{\mathrm{Ob}y}$ – amplitudes moduli and phases of objects' beam components E_{Ob_x}, E_{Ob_y}.

The polarization ellipses of the object field under its propagation, are generally unknown, and the interferometric information extracted from both the horizontal and vertical channels helps to reproduce them. Here we do not provide the interferometric, but only polarization data. The simulated polarization ellipses of the object field for $\alpha = 20°$ is shown in Fig. 3.

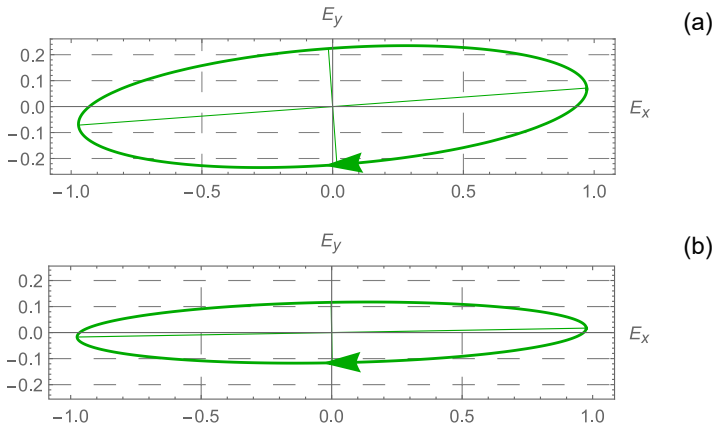

Fig. 3. (a) Polarization ellipse of the object field obtained after interaction of a linearly polarized beam $\begin{pmatrix} 1 \\ 0 \end{pmatrix}$ with the birefringent object. (b) Polarization ellipse formed in the horizontal (vertical) arms of the interferometer, after the beamsplitter BS4 (see Fig. 1).

Presented polarization ellipses of the object field contain information about the object, namely about the orientation of its optical axis (collagen fiber), which can be recovered and analyzed in order to diagnose pathological changes in the object.

Propagation of the object beam through the beamsplitter BS4, determines no changes in phase and polarization in the vertical arm of the interferometer and a jump in phase by π in horizontal arm, due to the reflection from the beamsplitter.

The propagation of the reference beam $\mathbf{E}_0 = \begin{pmatrix} 1 \\ 0 \end{pmatrix}$ is controlled by the beamsplitters BS1, BS2, BS4 and formed by reflection from the mirror M (Fig. 1). As a result, behind the beamsplitter BS4, in the vertical arm of the interferometer, the beam acquires a phase jump by π, and the beam remains unchanged in the horizontal arm. We use the horizontal arm of the interferometer to recover the initial horizontal polarization and to extract information about the geometric phase. In the vertical channel, the resulting polarization is formed by superposition of the object beam and the beam with modified initial horizontal polarization.

The polarization ellipses formed in the horizontal and vertical arms of the interferometer are identical (Fig. 3(b)).

In order to extract information from the interference signal about the phase delay δ (or dynamic phase), determined by the object thickness, it is required to have y-components of the superposing beams. For this purpose, we introduce an additional half -wave plate (HWP), placing it in front of the beamsplitter BS4 and analyze the signal by the detector D2. The plate is oriented in such a way as to form an angle of 45° between the fast axis of the HWP and the horizontal direction. Then the initial horizontal polarization $\mathbf{E}_0 = \begin{pmatrix} 1 \\ 0 \end{pmatrix}$ is transformed into $\mathbf{E}_0 = \begin{pmatrix} 1 \\ 0 \end{pmatrix}$. After that the transformed beam acquires a phase jump by π at the reflection by the BS4, and then superposes with the object beam.

To calculate the geometric phase, the interference field obtained by the superposition of the object beam and the $\begin{pmatrix} 1 \\ 0 \end{pmatrix}$ beam is analyzed by the detector D1 with extracting the information about x-components of the beams.

We use the Poincaré sphere (Fig. 4) to form a closed loop by applying to the sphere all the polarization states obtained during input beam polarization transformations. To reproduce the polarization state on the Poincaré sphere, it is required to convert the Jones vector parameters into the Stokes vector parameters S_1, S_2, S_3 [17]. We indicate the initial horizontal polarization, the polarization ellipse of the object beam, and the polarization ellipse behind the beamsplitter BS4 in the horizontal channel – the result of superposition of the transformed object beam and reference beam with horizontal polarization.

According to the theory, developed by Pancharatnam [16], one can obtain the value of the geometric phase as: $\varphi_G = \Omega_{123}/2$ (or $\varphi_G = \pi - \Omega_{123'}/2$, where $3'$ – the antipodal point for 3) from a spherical triangle on a Poincaré sphere (indicated by a dashed line in Fig. 4). Here Ω_{123} – the solid angle at which the spherical triangle 123 is viewed

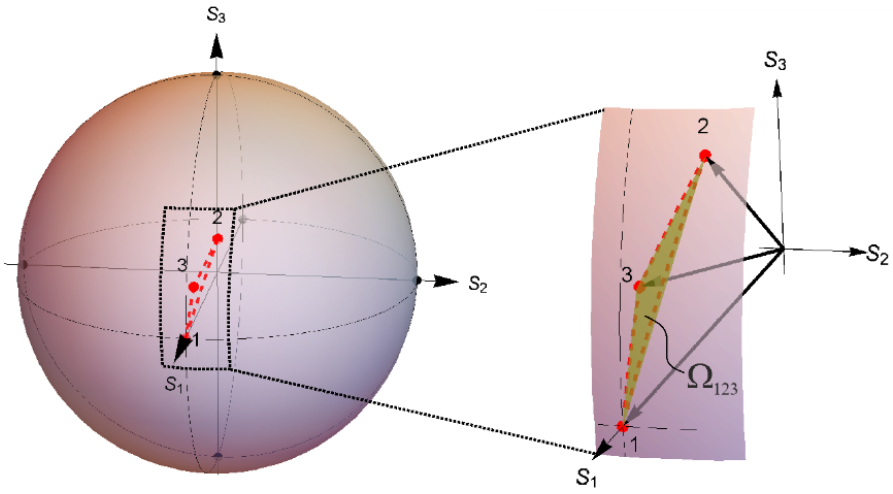

Fig. 4. Poincaré sphere with plotted polarization states during polarization transformation of a linear horizontally polarized beam: 1 – initial polarization state, 2 – polarization state of the object beam, 3 – polarization state due to superposition of the object and reference beams in the horizontal channel. Magnified region shows the spherical triangle 123 and the solid angle Ω_{123} used in calculations.

from the center of the sphere. For the provided geometric construction it is obtained: $\varphi_G = 16.7351°$.

To determine the medium parameters, let's consider the analytical description of the geometric phase, obtained from the Eq. (6). The total phase in the horizontal channel, due to the interference of x-components of object and reference beams is determined by the scalar product [8,16]:

$$\varphi_{hor} = \arg(E_{Ob_x} \cdot E_0 e^{-i\varphi_0}) = \varphi_D + \varphi_G - \varphi_0 \tag{7}$$

where $\varphi_D = 2\delta$ – a dynamic phase, $\varphi_G = \arctan(\tan\gamma \cos 2\alpha)$ – a geometric phase [8], from which the information about the birefringent medium can be extracted, $\varphi_0 = 2kz_0$ – the reference beam phase, where z_0 is the reference beam pathlength.

In the vertical channel, in a case of y-components superposition, the total phase is

$$\varphi_{ver} = \arg(E_{Ob_y} \cdot E_0 e^{i\pi} e^{-i\varphi_0}) = 2\delta + \frac{\pi}{2} - \varphi_0 = \varphi_D + \frac{\pi}{2} - \varphi_0 \tag{8}$$

and is determined by the dynamic phase, shifted by $\pi/2$ at the special experimental conditions.

The thickness of the sample is extracted from the dynamic phase, that is $d = \varphi_D/(2k\bar{n})$. The geometric phase, at a known value of $\gamma = k\Delta n d$, allows us to calculate $\alpha = 0.5 \arccos(\tan\varphi_G \cot\gamma)$. The orientation of the optical axis (collagen fibers) is estimated with respect to the horizontal direction, which removes the uncertainty in the choice of the value of α. Moreover, we take into account that the slow axis is oriented along the collagen fibers [4], the angle α sets the orientation of the fast axis of the

birefringent medium, then the fiber orientation is defined as $(\alpha + \pi/2)$ relative to the horizontal direction. In our case, it is obtained: $\varphi_D = 40.66$, $\gamma = 21.43°$, and the orientation of the collagen fibers is $\alpha + \pi/2 = 110°$.

4. Influence of structural changes in thin surface (subsurface) layers on the accuracy of restoring of biological anisotropic objects properties

The next step of the investigation is the analyze of a modified structure of the surface layer of the object (Fig. 2(b)) of thickness d_1, that is much less than the axial resolution of the system. The deeper subsurface layer of thickness $d_2 = d - d_1$ remains unchanged by its structure. To obtain the resulting interferometric signal from the object, consider the following approximation. Assume that the collagenous structure in a surface layer is broken and characterized by two angles of orientation (Fig. 2(b)): α_1 – the angle of orientation of collagen fibers in a plane of lamella surface with respect to the horizontal direction and β is the rotation angle of this plane relative to the orientation of unchanged lamella subsurface. The subsurface (unchanged) layer is characterized only by angle α_2 of optical axis orientation. In this case, refractive indices of surface and subsurface layers differ, and Fresnel reflection will occur at the interfaces. In approximation of small Δn values, the mean refractive index and birefringence of surface layer will be dependent on β [13]:

$$n_1(\beta) = \frac{n_0}{2}\left(1 + \frac{n_e}{\sqrt{n_o^2\cos^2\beta + n_e^2\sin^2\beta}}\right) \tag{9a}$$

$$\Delta n_1(\beta) \approx (n_e - n_o)\cos^2\beta \tag{9b}$$

Fresnel reflection coefficients (in a case of small Δn) at surface layer interfaces are:

$$r_1 = \frac{|n_1(\beta) - n_{base}|}{|n_1(\beta) + n_{base}|} \tag{10a}$$

$$r_2 = \frac{|\overline{n} - n_1(\beta)|}{|\overline{n} + n_1(\beta)|} \tag{10b}$$

Let's consider interference signals in a horizontal and verticals channels, formed by the surface layer. In this case, the interference signal for x-components will be a sum of interferograms, obtained for the reflected waves from first and second interfaces: $I_x = I_{1x} + I_{2x}$, which can be written in the following form (without taking into account the constant component of the signals) [18]: $I_{1x} = \varepsilon_{1x}\cos\Phi_{1x}$, $I_{2x} = \varepsilon_{2x}\cos\Phi_{2x}$. Here ε_{1x}, ε_{2x} – amplitudes and Φ_{1x}, Φ_{2x} – phases of interferograms, which, in general, are the functions of the optical path length z_0 (or phase φ_0) of the reference beam. These values can be described as follows:

$$\varepsilon_{1x} = 2A_0 A_{1x} \Gamma(\Delta z_1) \tag{11a}$$

$$\varepsilon_{2x} = 2A_0 A_{2x} \Gamma(\Delta z_2) \tag{11b}$$

$$\Phi_{1x} = \varphi_{1x} - \varphi_0 \tag{11c}$$

$$\Phi_{2x} = \varphi_{2x} - \varphi_0 \tag{11d}$$

where

$$A_0 = E_0$$

$$A_{1ax} = E_0 r_1$$

$$A_{2x} = E_0 (1 - r_1)^2 r_2 \sqrt{\cos^2\gamma_1 + \sin^2\gamma_1 \cos^2 2\alpha_1}$$

$$\Delta z_1 = z_0 - n_{\text{base}} z_1$$

$$\Delta z_2 = z_0 - n_1 z_{1b}$$

$$\varphi_{1x} = \pi,\ \varphi_{2x} = \pi + \varphi_{\text{D1}} + \varphi_{\text{G1}} = \pi + 2kn_1 d_1 + \arctan(\tan\gamma_1 \cos 2\alpha_1)$$

$$\gamma_1 = k\Delta n_1 d_1$$

$$\Gamma(\Delta z_{1,2}) = \exp(-4\ln 2\, \Delta z_{1,2}^2 / l_c^2)$$

Then the resulting x-interference signal can be written as: $I_x = \varepsilon_x \cos\Phi_x$, the amplitude ε_x and phase Φ_x will be expressed in terms of amplitudes and phases of both interferograms [18]:

$$\varepsilon_x = \sqrt{\varepsilon_{1x}^2 + \varepsilon_{2x}^2 + 2\varepsilon_{1x}\varepsilon_{2x}\cos(\Phi_{1x} - \Phi_{2x})} \tag{12}$$

$$\tan\Phi_x = \frac{\varepsilon_{1x}\sin\Phi_{1x} + \varepsilon_{2x}\sin\Phi_{2x}}{\varepsilon_{1x}\cos\Phi_{1x} + \varepsilon_{2x}\cos\Phi_{2x}} \tag{13}$$

The y-component of the interference signal will be formed only for the wave reflected from the second (inner) interface of the surface layer, since the incident wave is x-polarized. Then the y-interferogram for the surface layer can be written as

$$I_y = = \varepsilon_y \cos\Phi_y \tag{14}$$

where the amplitude and phase respectively determined as:

$$\varepsilon_y = 2A_0 A_y \Gamma(\Delta z_2)$$

$$\Phi_y = \varphi_y - \varphi_0.$$

Here $A_y = (1 - r_1) r_2 \sin\gamma_1 \sin 2\alpha_1$, $\varphi_y = \pi + \pi/2 + \varphi_{\text{D1}} = 3\pi/2 + 2kn_1 d_1$.

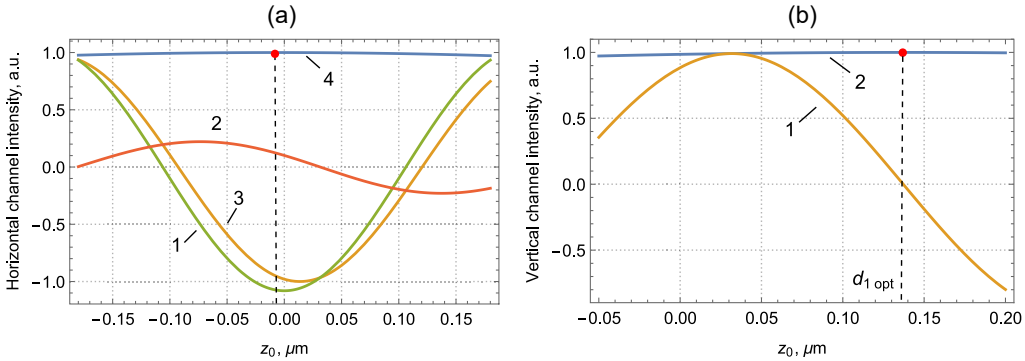

Fig. 5. Interferograms obtained for (a) x- and (b) y-components of surface layer object field with a change of a reference beam path length z_0: (a) curve 1 – I_{1x}, curve 2 – I_{2x}, curve 3 – I_x, curve 4 – envelope of I_x; (b) curve 1 – I_y, curve 2 – envelope of I_y. Red point indicates the maximum value position of interferogram envelopes.

Resulting x- and y-interferograms (normalized to its envelope maximum values) obtained in a case of $\alpha_1 = 30°$, $\beta = 30°$, $d_1 = 0.1$ μm are presented in Fig. 5.

According to presented results, the surface layer diagnostics may be done with respect to the position of envelopes maxima of x- and y-interferograms, which are different. Maximum of the y-interferogram envelope gives the position z_0 which corresponds to the optical thickness of layer $n_1 d_1$ (Fig. 5(b)). At the same time, the position of maximum of the of x-interferogram envelope is shifted, and does not correspond to the positions of either the first or the second surfaces (Fig. 5(a)). Also, the x-interferogram phase is different from π for $z_0 = 0$.

In general, three parameters of surface layer are unknown: α_1, β and d_1. Let the zero position of the beam be associated with the position of the first (upper) surface, $z_1 = 0$, then the next position of the beam on the second (inner) surface depends on the geometric thickness of the layer: $z_2 = d_1$. Estimation of the amplitude and phase of resulting interferograms will be carried out for the reference arm path length, which corresponds to the optical thickness of the layer: $z_0 = n_1 d_1 = d_{1\,\mathrm{opt}}$, the value of which is obtained from the y-interferogram. The amplitude of x-interferogram $\varepsilon_x(d_{1\,\mathrm{opt}})$ is a function of d_1 and β_1, and y-interferogram amplitude $\varepsilon_y(d_{1\,\mathrm{opt}})$ depends on angle α_1.

To simplify the procedure of searching for unknown parameters, we use the following approximation. As we know, that $n_o < n_1(\beta) < \overline{n}$, the approximated geometric thickness of the surface layer $\tilde{d}_1$ can be estimated as $d_{1\,\mathrm{opt}}/n_o < \tilde{d}_1 < d_{1\,\mathrm{opt}}/\overline{n}$. Then the "optimization approach" can be solved as follows: a search of solutions of β for a given range of $\tilde{d}_1$, by minimizing error of Eq. (10).

The obtained results are quite successful, even if $\tilde{d}_1 \approx d_{1\,\mathrm{opt}}$. At this case, it is obtained that $\beta = 29.816°$, with an error of Eq. (10): $\Delta = 9 \times 10^{13}$ a.u. The refractive index of the surface layer by using the obtained value of β can be calculated from Eq. (8): $n_1(\beta) = 1.37166$, and the geometric thickness can be clarified: $d_1 = d_{1\,\mathrm{opt}}/n_1(\beta) =$

= 0.0999 μm. The obtained values of β and d_1 allow to calculate Δn_1 with Eq. (8), then $\gamma_1 = k\Delta n_1 d_1$ and the parameter α_1 can be found from Eq. (13). Thus $\Delta n_1 = 0.0189$, $\gamma_1 = 0.014$ and $\alpha_1 = 30.34°$. Errors of the restored parameters of the surface layer are $\delta\beta = 0.6\%$, $\delta\alpha_1 = 1.12\%$, and $\delta\gamma_1 = 0.38\%$.

The known surface layer parameters allow us to extract information about the subsurface layer's object field polarization and restore the whole medium properties using the procedure prescribed previously. For our case, if the surface layer is not taken into consideration, the error of restored parameter α_2 is about 4.4%. Information about nanosized modified (changed, destroyed) surface layer obtained with our approach, increase the accuracy up to 98.99% of restoring the whole lamella parameters of the anisotropic object, which is impossible to perform by existing PS-OCT.

5. Conclusions

Paper presents new results obtained by computer simulation of polarization-sensitive optical coherence tomography of thin surface (subsurface) layers of birefringent biological tissue. Extracting the geometric phase of the object field in a modified Mach –Zehnder interference scheme enables to obtain the information about the medium polarization structure (optical axis orientation). Method of determination the parameters of nanosized-thickness surface layers is proposed. Taking into account the surface layer information allows to increase the accuracy both of subsurface layer and whole volume parameters recovering in non-invasive way, which is difficult for the existing PS-OCT approaches.

References

[1] Drexler W., Fujimoto J.G. [Eds.], *Optical Coherence Tomography*, Springer, Cham 2015: 2571. https://doi.org/10.1007/978-3-319-06419-2

[2] Everett M., Magazzeni S., Schmoll T., Kempe M., *Optical coherence tomography: From technology to applications in ophthalmology*, Translational Biophotonics **3**(1), 2021: e202000012. https://doi.org/10.1002/tbio.202000012

[3] Pircher M., Hitzenberger C.K., Schmidt-Erfurth U., *Polarization sensitive optical coherence tomography in the human eye*, Progress in Retinal and Eye Research **30**(6), 2011: 431-451. https://doi.org/10.1016/j.preteyeres.2011.06.003

[4] Baumann B., *Polarization sensitive optical coherence tomography: A review of technology and applications*, Applied Sciences **7**(5), 2017: 474. https://doi.org/10.3390/app7050474

[5] Pierce M.C., Shishkov M., Hyle Park B., Nassif N.A., Bouma B.E., Tearney G.J., de Boer J.F., *Effects of sample arm motion in endoscopic polarization-sensitive optical coherence tomography*, Optics Express **13**(15), 2005: 5739–5749. https://doi.org/10.1364/OPEX.13.005739

[6] Jisha C.P., Nolte S., Alberucci A., *Geometric phase in optics: From wavefront manipulation to waveguiding*, Laser & Photonics Reviews **15**(10), 2021: 2100003. https://doi.org/10.1002/lpor.202100003

[7] Dou J., Xi T., Ma C., Di J., Zhao J., *Measurement of full polarization states with hybrid holography based on geometric phase*, Optics Express **27**(6), 2019: 7968-7978. https://doi.org/10.1364/OE.27.007968

[8] KURZYNOWSKI P., WOŹNIAK W.A., SZARYCZ M., *Geometric phase: Two triangles on the Poincaré sphere*, Journal of the Optical Society of America A **28**(3), 2011: 475-482. https://doi.org/10.1364/JOSAA.28.000475

[9] BRON A.J., *The architecture of the corneal stroma*, British Journal of Ophthalmology **85**(4), 2001: 379–381. https://doi.org/10.1136/bjo.85.4.379

[10] TUCHIN V.V., *Tissue Optics: Light Scattering Methods and Instruments for Medical Diagnostics*, Third Ed., SPIE, Bellingham 2015: 988. https://doi.org/10.1117/3.1003040

[11] MEEK K.M., KNUPP C., *Corneal structure and transparency*, Progress in Retinal and Eye Research **49**, 2015: 1–16. https://doi.org/10.1016/j.preteyeres.2015.07.001

[12] DONOHUE D.J., STOYANOV B.J., MCCALLY R.L., FARRELL R.A., *Numerical modeling of the cornea's lamellar structure and birefringence properties*, Journal of the Optical Society of America A **12**(7), 1995: 1425-1438. https://doi.org/10.1364/JOSAA.12.001425

[13] YANG B., JAN N.J., BRAZILE B., VOORHEES A., LATHROP K.L., SIGAL I.A., *Polarized light microscopy for 3-dimensional mapping of collagen fiber architecture in ocular tissues*, Journal of Biophotonics **11**(8), 2018: e201700356. https://doi.org/10.1002/jbio.201700356

[14] LIPPOK N., COEN S., LEONHARDT R., NIELSEN P., VANHOLSBEECK F., *Instantaneous quadrature components or Jones vector retrieval using the Pancharatnam–Berry phase in frequency domain low-coherence interferometry*, Optics Letters **37**(15), 2012: 3102-3104. https://doi.org/10.1364/OL.37.003102

[15] LIPPOK N., COEN S., LEONHARDT R., NIELSEN P., VANHOLSBEECK F., *Depth-ambiguity free or polarization sensitive optical frequency domain imaging using the Pancharatnam-Berry phase*, Proceedings of the SPIE, Vol. 8213, Optical Coherence Tomography and Coherence Domain Optical Methods in Biomedicine XVI, 2012: 82131J. https://doi.org/10.1117/12.911632

[16] GARZA-SOTO L., HAGEN N., LOPEZ-MAGO D., *Deciphering Pancharatnam's discovery of geometric phase: Retrospective*, Journal of the Optical Society of America A **40**(5), 2023: 925-931. https://doi.org/10.1364/JOSAA.485485

[17] COLLETT E., *Field Guide to Polarization*, SPIE Press, Bellingham 2005: 7-61. https://doi.org/10.1117/3.626141

[18] GARZA-SOTO L., HAGEN N., LOPEZ-MAGO D., OTANI YU., *Wave description of geometric phase*, Journal of the Optical Society of America A **40**(2), 2023: 388-396. https://doi.org/10.1364/JOSAA.480814

Received October 14, 2023